HHS Public Access

Author manuscript

Nat Chem Biol. Author manuscript; available in PMC 2013 September 01.

Published in final edited form as:

Nat Chem Biol. 2013 March ; 9(3): 163–168. doi:10.1038/nchembio.1166.

PUMA Binding Induces Partial Unfolding within BCL-xL to Disrupt p53 Binding and Promote Apoptosis

Ariele Viacava Follis[1,*], **Jerry E. Chipuk**[2,#,*], **John C. Fisher**[1,4,*], **Mi-Kyung Yun**[1], **Christy R. Grace**[1], **Amanda Nourse**[3], **Katherine Baran**[2], **Li Ou**[1], **Lie Min**[1], **Stephen W. White**[1,5], **Douglas R. Green**[2,6,**], and **Richard W. Kriwacki**[1,5,6,**]

[1]Department of Structural Biology, St. Jude Children's Research Hospital, 262 Danny Thomas Place, Memphis, Tennessee, USA 38105

[2]Department of Immunology, St. Jude Children's Research Hospital, 262 Danny Thomas Place, Memphis, Tennessee, USA 38105

[3]Hartwell Center for Bioinformatics and Biotechnology, St. Jude Children's Research Hospital, 262 Danny Thomas Place, Memphis, Tennessee, USA 38105

[4]College of Medicine, University of Tennessee Health Sciences Center, Memphis, Tennessee, USA 38163

[5]Department of Microbiology, Immunology and Biochemistry, University of Tennessee Health Sciences Center, Memphis, Tennessee, USA 38163

Abstract

Following DNA damage, nuclear p53 induces the expression of PUMA, a BH3-only protein that binds and inhibits the anti-apoptotic BCL-2 repertoire, including BCL-xL. PUMA, unique amongst BH3-only proteins, disrupts the interaction between cytosolic p53 and BCL-xL, allowing p53 to promote apoptosis via direct activation of the BCL-2 effector molecules, BAX and BAK. Structural investigations using nuclear magnetic resonance spectroscopy and X-ray crystallography revealed that PUMA binding induced partial unfolding of two α-helices within BCL-xL. Wild-type PUMA or a PUMA mutant incapable of causing binding-induced unfolding of BCL-xL equivalently inhibited the anti-apoptotic BCL-2 repertoire to sensitize for death receptor (DR)-activated apoptosis, but only wild-type PUMA promoted p53-dependent, DNA damage-induced apoptosis. Our data suggest that PUMA-induced partial unfolding of BCL-xL disrupts interactions between cytosolic p53 and BCL-xL, releasing the bound p53 to initiate apoptosis. We

[6]Corresponding authors information: D.R.G.: phone (901) 595-3488, douglas.green@stjude.org. R.W.K.: phone (901) 595-3290, richard.kriwacki@stjude.org.

[#]Current Affiliations: Mount Sinai School of Medicine, Departments of Oncological Sciences and Dermatology, The Tisch Cancer Institute, One Gustave L. Levy Place, Box 1130, New York, New York 10029

[*,**]These authors contributed equally.

Author Contributions:

A.V.F. performed experiments, analyzed data and wrote the paper; J.E.C. performed experiments, analyzed data and wrote the paper; J.C.F. performed experiments, analyzed data and wrote the paper; M-K,Y., C.R.G., A.N., K.B., L.O., and L.M. performed experiments and analyzed data; and S.W.W., D.R.G. and R.W.K analyzed data and wrote the paper.

propose that regulated unfolding of BCL-xL provides a mechanism to promote PUMA-dependent signaling within the apoptotic pathways.

In several tissues, DNA-damage induces apoptosis via the stabilization of p53, which accumulates in the nucleus and cytosol[1]. While cytosolic p53 is sequestered by the anti-apoptotic BCL-2 family protein BCL-xL[1,2], nuclear p53 induces the expression of a large number of proteins, including PUMA[3–5]. PUMA potently binds and inhibits the anti-apoptotic BCL-2 proteins[6,7] and is required for DNA damage-induced apoptosis[5]. PUMA is a BH3-only protein and acts as a key mediator of cytosolic pro-apoptotic p53 function by freeing cytosolic p53 from inactive complexes with BCL-xL. No other BH3-only protein is capable of efficiently releasing p53 from BCL-xL[2]. Upon release from BCL-xL, cytosolic p53 can directly activate BAX or BAK, thereby triggering the apoptotic signaling cascade via mitochondrial outer membrane permeabilization (MOMP)[8,9]. Thus, PUMA effectively couples the nuclear (transcriptional) and cytosolic pro-apoptotic functions of p53[1,2,10] (Fig. 1a). We therefore sought a biochemical and structural mechanism for this unique property of PUMA.

Our studies revealed that PUMA was an intrinsically disordered protein and that its BH3 domain folded upon binding within the hydrophobic of BCL-xL. Many of the interactions between PUMA and BCL-xL involved residues conserved in BH3 domains and BCL-2 family proteins, respectively. However, tryptophan 71 (Trp^{71}) of PUMA, unique at this position amongst BH3 domains, specifically interacted with histidine 113 (His^{113}) of BCL-xL through a π-stacking interaction and this interaction was associated with partial unfolding of α-helixes 2 and 3 (of BCL-xL). PUMA binding-induced partial unfolding of BCL-xL abrogated binding to p53, providing a mechanism for PUMA-induced activation of cytosolic p53-dependent MOMP and apoptosis. The interaction between Trp^{71} (of PUMA) and His^{113} (of BCL-xL) was demonstrated to be necessary for partial unfolding of BCL-xL, abrogation of p53 binding, permeabilization of the outer membranes of isolated mitochondria and p53-dependent apoptosis in cells.

Results

The intrinsically disordered PUMA BH3 domain binds BCL-xL

Circular dichroism (CD) and NMR indicated that PUMAβ, the smallest of two splicing variants containing a functional BH3 domain[3–5,10] (hereafter called PUMA), was intrinsically disordered (Supplementary Results, Supplementary Fig. 1a, b), as observed for other BH3-only proteins[11]. We studied the beta isoform of PUMA because we could not express the alpha isoform in *E. coli* (data not shown); the two isoforms are equipotent in inducing p53-dependent apoptosis[3,10]. Both isothermal titration calorimetry (ITC) and NMR showed that the BH3 domain of PUMA ($PUMA^{BH3}$) was the principal site of interaction with BCL-xL, as previously reported[6,7,10] (Supplementary Fig. 2a–c). These analyses did not identify significant differences between the BCL-xL·PUMA complex and similar BH3 domain-bound BCL-xL complexes that have been structurally characterized[12–15]. A conserved motif within disordered BH3 domains (Fig. 1b) adopts an amphipathic, α-helical conformation and exhibits conserved binding interactions within a hydrophobic groove of

BCL-2 family members; residues flanking the BH3 motif also contribute to these interactions[12–15]. However, comparison of these motifs and flanking regions within different complexes provided no obvious structural basis for the unique ability of PUMA to release p53 from BCL-xL. While cytosolic p53 exhibits the functional features of a direct activator BH3-only protein[8], its sequence lacks a canonical BH3 domain. Rather, a broad, positively charged surface of the DNA binding domain binds to an acidic surface of BCL-xL that does not overlap with its BH3 binding groove[16,17]. Therefore, it appeared unlikely that PUMA would directly compete for the p53-binding site on BCL-xL.

PUMA binding induces unfolding of BCL-xL α-helix 3

To understand the mechanism by which PUMA releases p53 from BCL-xL, we determined the NMR solution structure of the complex of BCL-xLΔLΔC and PUMA^{BH3} (Fig. 1c and Supplementary Table 1). BCL-xLΔLΔC is a functional BCL-xL protein lacking the unstructured loop connecting α-helix 1 (α1) to α2 as well as the C-terminal 22 residues[18]. We used this construct for NMR experiments because intense resonances of the disordered loop overlap and interfere with those of the folded BCL-xL core. The α1-α2 loop was, however, present in the BCL-xLΔC construct, lacking only the C-terminal 22 residues[18], used for other functional assays. We found that PUMA^{BH3} bound within the hydrophobic groove of BCL-xLΔLΔC (Fig. 1c) similarly to other BCL-xL·^{BH3} domain complexes[12–15]. Strikingly, however, PUMA^{BH3} extensively perturbed resonances of residues within α2 and α3 of ^{15}N-BCL-xLΔLΔC, and, to a smaller extent, those within α4 (Fig. 1d). Furthermore, in contrast to other well-structured regions of BCL-xL, the α3 region displayed weak ^{1}H-^{1}H NOE correlations and was poorly defined in our solution structure (Fig. 1c). In contrast, the binding of the BH3 domain of BAD (BAD^{BH3}) caused more subtle chemical shift perturbations in the same regions of ^{15}N-BCL-xLΔLΔC (Fig. 1e) consistent with simple complex formation. These observations suggested that the binding of PUMA^{BH3} enhanced the dynamics of the α2-α3 region of BCL-xLΔLΔC. We then analyzed polypeptide backbone flexibility using the random coil index order parameter (RCI S^2)[19], and this confirmed that the binding of PUMA^{BH3} enhanced disorder within the α2-α3 region of BCL-xLΔLΔC, in contrast to the high degree of order observed for apo BCL-xLΔLΔC and the BCL-xLΔLΔC·BAD^{BH3} complex (Fig. 1f). We directly analyzed polypeptide dynamics on the ps to ns timescale through measurement of the {^{1}H}-^{15}N heteronuclear nuclear Overhauser effect (HetNOE) for backbone amide groups. The binding of PUMA^{BH3} dramatically enhanced dynamics within BCL-xLΔLΔC, as evidenced by reduced HetNOE values in the α2-α3 region, while these values for apo BCL-xLΔLΔC and the BCL-xLΔLΔC·BAD^{BH3} complex reflected far less flexibility (Fig. 1g). These results suggested that the binding of PUMA caused partial unfolding of α2 and α3 within BCL-xL.

PUMA Trp^{71} engages in π–stacking with BCL-xL His^{113}

To gain more insights into the structure of the BCL-xL·PUMA complex, we co-crystallized BCL-xLΔC (a functional BCL-xL protein lacking the carboxyl terminal 22 residues)[18] with PUMA^{BH3} and determined the structure to 2.9 Å resolution (Supplementary Table 2). In contrast to the 1:1 stoichiometry of the NMR-derived structure, the BCL-xLΔC ·PUMA^{BH3} complex crystallized in a domain-swapped, dimeric structure with 2:2 stoichiometry in which α6-α8 of one BCL-xLΔC molecule replaced α6′-α8′ of the symmetry mate (Fig. 2a

and Supplementary Fig. 3). A similar oligomeric form was previously observed for apo BCL-xLΔC either through alkaline[20] or heat treatment[21], suggesting that our dimeric crystal structure was a crystallization artifact resulting from the binding of PUMA^{BH3}. We confirmed the NMR-observed 1:1 stoichiometry of the BCL-xLΔC ·PUMA^{BH3} complex in solution using analytical ultracentrifugation (Supplementary Tables 3, 4; Supplementary Fig. 4a, b). In addition, we recorded 2D ^{1}H-^{15}N TROSY spectra of monomeric and heat-induced, dimeric BCL-xLΔLΔC[21] to which one or two molar equivalents of PUMA^{BH3} per BCL-xL monomer or dimer were added, respectively. The spectrum of the 2:2 dimeric BCL-xLΔLΔC ·PUMA^{BH3} complex exhibited many chemical shift differences in comparison with that of the 1:1 monomeric complex (Supplementary Fig. 4c). Finally, native polyacrylamide gel electrophoresis (PAGE) clearly demonstrated that the 1:1 BCL-xL·PUMA^{BH3} complex is the predominant species in solution (Supplementary Fig. 4d) and also PUMA-associated BCL-xL immunoprecipated from UV-treated MCF7 cells was exclusively monomeric with 1:1 stoichiometry (Supplementary Fig. 4e, f).

With the exception of the oligomeric states, however, the solution and crystallographic structures of the globular core of BCL-xL were very similar (backbone atom r.m.s.d. value of 2.1 Å). The PUMA^{BH3} binding site appeared to be minimally affected by dimerization, and we therefore analyzed the interactions between PUMA^{BH3} and the hydrophobic groove of BCL-xLΔC within the crystal structure. The interface exhibited many of the interactions observed in other BCL-xL·^{BH3} domain structures (Supplementary Fig. 5a), although interactions between PUMA^{BH3} and the α3 helix of BCL-xLΔC were less extensive than observed in the BCL-xLΔC·BAD^{BH3} complex (Supplementary Fig. 5b, c). A notable unique feature of the BCL-xLΔC ·PUMA^{BH3} complex was that BCL-xLΔC Pro^{116}, located in the loop between α3 and α4, was markedly displaced by approximately 5 Å relative to its position in apo BCL-xL and other BCL-xLΔBH3 domain structures (Supplementary Fig. 6a–d)[12–15,20]. An adjacent π-stacking interaction between the aromatic side chains of PUMA^{BH3} Trp^{71} and BCL-xLΔC His^{113} appeared to induce this conformational change (Fig. 2a). We also observed these structural features in the solution structure of the BCL-xLΔLΔC·PUMA^{BH3} complex (Fig. 1c and Supplementary Fig. 6b–d). Trp^{71} of PUMA is unique amongst the flanking sequences of BH3 domains (Fig. 1b), and its interfacial interaction occurred proximal to the region of BCL-xL shown by NMR to experience enhanced dynamics upon PUMA^{BH3} binding. PUMA binding did not induce similar structural perturbations associated with Trp^{71} in complexes of PUMA^{BH3} with other anti-apoptotic BCL-2 proteins, including MCL-1 and A1[22,23] (Supplementary Fig. 6e). In summary, our NMR and X-ray results suggested that the binding of PUMA specifically perturbed the structure of and induced partial unfolding within BCL-xL. Moreover, Trp^{71}, unique to the BH3 domain of PUMA, played a critical role in mediating these structural and dynamic perturbations via π-stacking with His^{113} of BCL-xL.

PUMA Trp^{71} mediates release of p53 from BCL-xL in vitro

To test whether our structural conclusions represented the mechanistic basis for PUMA's biological role in releasing p53 from its complex with BCL-xL, we probed the ability of a panel of BH3 domain peptides to disrupt the interaction between BCL-xLΔC and p53. For binding assays, we used a near full-length, stable mutant of p53 (human p53 residues 1-360

with Met^{133} mutated to Leu, Val^{203} to Ala, and Asn^{268} to Asp; p53^{SM} 1-360)[24,25]. The mutated residues are located within the core of the DNA binding domain; the mutations thermodynamically stabilize this domain but do not significantly affect its structure or DNA binding function[24,25]. p53^{SM} 1-360 was used in these assays to overcome the intrinsic instability of the wild-type sequence[24] and because the N-terminal[26] and DNA binding domains[16,17], but not the C-terminal domain (of p53), have been reported to interact with BCL-xL. Fluorescence polarization measurements showed that p53^{SM} 1-360 bound with approximately equal affinity to fluorescently-labeled apo BCL-xLΔC (F-BCL-xLΔC) as well as to F-BCL-xLΔC pre-incubated with all BH3 domain peptides except PUMA^{BH3} (Fig. 1b, Fig. 2b, Supplementary Fig. 7). However, pre-incubation of F-BCL-xLΔC with a PUMA^{BH3} peptide in which Trp^{71} was substituted with Ala (PUMA$^{BH3\ W\rightarrow A}$) restored F-BCL-xLΔC binding to p53^{SM} 1-360 (Fig. 2b). Importantly, PUMA$^{BH3\ W\rightarrow A}$ bound to BCL-xLΔC with a K_D value identical to that of wild-type PUMA^{BH3} (Supplementary Table 5). Similarly, a mutant form of BCL-xL in which His^{113} was substituted with Ala (BCL-xLΔC $^{H\rightarrow A}$) was able to compete with wild-type F-BCL-xLΔC for p53 binding in the apo form and when bound to PUMA^{BH3} (Supplementary Fig. 8a). The affinity of BCL-xLΔC$^{H\rightarrow A}$ for p53 was reduced 10-fold relative to wild-type BCL-xLΔC (Supplementary Fig. 8a); however, this affinity was unaffected by pre-incubation with PUMA^{BH3}. Furthermore, the affinity of BCL-xLΔC$^{H\rightarrow A}$ for PUMA^{BH3} was similar to that of wild-type BCL-xLΔC (Supplementary Fig. 8b), as was also observed with PUMA$^{BH3\ W\rightarrow A}$. We did not observe the partial unfolding of BCL-xLΔLΔC induced by wild-type PUMA^{BH3} either with PUMA$^{BH3\ W\rightarrow A}$ or in the complex of BCL-xLΔLΔC $^{H\rightarrow A}$ with wild-type PUMA^{BH3} (Fig. 2c and Supplementary Fig. 9). Finally, NMR chemical shift perturbations induced within ^{15}N-BCL-xLΔLΔC by p53 binding (Supplementary Fig. 10) were absent when BCL-xLΔLΔC was pre-incubated with PUMA^{BH3} (Fig. 2d) but were observed upon pre-incubation with PUMA$^{BH3\ W\rightarrow A}$ (Fig. 2e), BAD^{BH3} or BID^{BH3} (Supplementary Fig. 11). Similarly, the addition of p53^{SM} 1-360 to ^{15} N-BCL-xLΔLΔC $^{H\rightarrow A}$ pre-incubated with PUMA^{BH3} exhibited similar chemical perturbations indicative of p53 binding (Fig. 2f). These results indicated that Trp^{71} of PUMA and His^{113} of BCL-xL were required for PUMA binding-dependent release of p53 from BCL-xL but that the interaction of these two residues, while critical for p53 release, was not required for PUMA to bind BCL-xL with high affinity.

Importantly, p53 bound with equal affinity to and caused similar chemical shift perturbations within BCL-xLΔLΔC and BCL-xLΔC (Supplementary Figs. 10 and 12). This finding, along with the ability of PUMA to equally disrupt p53 binding to BCL-xLΔC or BCLxLΔLΔC [measured by fluorescence polarization (Fig. 2b) or NMR (Fig. 2d), respectively], strongly suggested that the α1-α2 loop of BCL-xL was not a major contributor to p53 binding or to its release through binding of PUMA. Collectively, our NMR-based results demonstrated that the binding of PUMA specifically induced unfolding within the α2-α3 region of BCL-xL, which, in turn, disrupted interactions with p53^{SM} 1-360. As mentioned above, the binding site on BCL-xL for PUMA does not overlap with that for p53 (Fig. 2g and Supplementary Figs. 10 and 12). Published[16,17] as well as our own NMR chemical shift perturbation data (Supplementary Figs. 10 and 12) indicate that the DNA binding domain of p53 interacts with the C terminus of α1, α3, and the loops between α3-α4

and α5-α6 of BCL-xL (Fig. 2g). We propose that PUMA acts via an allosteric mechanism involving local unfolding of α3 within BCL-xL that significantly disrupts its interface with p53.

PUMA Trp^{71} is required to activate cytosolic p53

We previously demonstrated that native, cytosolic p53 (immunopurified from UV irradiated MCF-7 cells, referred to as p53^{UVIP}) is bound and inhibited by BCL-xL, and that disruption of this complex by PUMA releases p53^{UVIP} to activate BAX and induce MOMP, as detected by the release of cytochrome c from mitochondria[2,8,10]. We therefore compared the ability of PUMA, PUMA^{BH3} and our panel of BH3 domain peptides to disrupt the BCL-xLΔC·p53^{UVIP} complex (Fig. 3a, b). BID^{BH3} and BIM^{BH3}, which bind to BCL-xLΔC with affinities similar to that of PUMA^{BH3} (Supplementary Table 5), failed to disrupt the BCL-xLΔC·p53^{UVIP} complex (Fig. 3a), as also observed for all other BH3 peptides except PUMA^{BH3} (Fig. 3b). In contrast, PUMA^{BH3} and PUMA both caused release of p53^{UVIP} from BCL-xLΔC. Further, we examined the ability of the released p53 to activate BAX and effect MOMP. Mitochondria lacking BAK and BAX (*bak*$^{-/-}$*bax*$^{-/-}$) did not undergo MOMP in response to caspase-8-activated BID (C8-BID), p53^{UVIP}, PUMA^{BH3}, PUMA or BAX alone, but released cytochrome c when exposed to BAX plus C8-BID or p53^{UVIP} (but not PUMA^{BH3} or PUMA) (Supplementary Fig. 13a), as described[10,27]. Addition of BCL-xLΔC in the presence of BAX and p53^{UVIP} inhibited MOMP; however, subsequent addition of PUMA or PUMA^{BH3}, but not the other BH3 peptides, promoted cytochrome c release (Fig. 3b) (This experiment was not performed with BIM or BID, as these BH3 domain peptides directly promote BAX-dependent MOMP)[27]. Although PUMA has been described to activate BAK and BAX directly[28,29], we have failed to observe this activity of any PUMA isoform or of PUMA^{BH3} peptides[10] (Supplementary Fig. 13a), and therefore cannot ascribe the effects of PUMA or PUMA^{BH3} to direct activation of BAX in this system.

We then examined the role of PUMA Trp^{71} in p53 release and MOMP (Fig. 3c). BAX-dependent MOMP associated with disruption of the BCL-xLΔC·p53^{UVIP} complex was observed with PUMA, PUMA^{BH3} and PUMA-BAD^{BH3} (a fusion peptide comprised of the N-terminal segment of PUMA^{BH3} containing Trp^{71} and the central conserved and C-terminal segment of BAD^{BH3}), but not with PUMA$^{BH3\ W\rightarrow A}$ or BAD^{BH3} (Fig. 3c). In contrast, PUMA, PUMA^{BH3}, PUMA$^{BH3\ W\rightarrow A}$, PUMA-BAD^{BH3} and BAD^{BH3} were all active in derepressing a complex of BCL-xL and C8-BID to promote BAX activation and MOMP (Supplementary Fig. 13b). The unique ability of PUMA to disrupt the BCL-xL·p53^{UVIP} complex could not be ascribed to differences in the affinity of these peptides for BCL-xL (Supplementary Table 5).

Overexpression of PUMA in cells can induce apoptosis[3], but low-level expression of PUMA, while not inducing apoptosis itself, can sensitize *PUMA*$^{-/-}$cells but not *p53*$^{-/-}$ cells to UV-induced apoptosis[2,8]. We therefore examined the ability of PUMA versus PUMA$^{W\rightarrow A}$ (PUMA in which Trp^{71} was mutated to Ala) to sensitize *p53*$^{-/-}$ and *puma*$^{-/-}$ MEFs (Supplementary Fig. 14a). While wild-type cells were sensitive to UV-induced apoptosis, *p53*$^{-/-}$ and *puma*$^{-/-}$ cells were not. Ectopic expression of PUMA sensitized *puma*$^{-/-}$ cells to UV, while PUMA$^{W\rightarrow A}$ was much less effective, and neither sensitized

p53$^{-/-}$ cells to UV. As expected, wild-type and *puma*$^{-/-}$ MEFs were equally susceptible to TNF-induced apoptosis, and ectopic expression of PUMA or PUMA$^{W\rightarrow A}$ equivalently sensitized cells for TNF-induced apoptosis (Fig. 4a and Supplementary Fig. 14b). In contrast, *p53*$^{-/-}$ or *puma*$^{-/-}$ MEFs were resistant to UV-induced apoptosis (Supplementary Fig. 14c), as described previously[2,8]. However, while ectopic expression of PUMA sensitized *puma*$^{-/-}$ MEFs to UV-induced apoptosis, PUMA$^{W\rightarrow A}$ was ineffective (Fig. 4b). Immunoprecipitation of PUMA or PUMA $^{W\rightarrow A}$ from these cells revealed that while both forms of PUMA co-precipitated BCL-xL, BCL-xL remained associated with p53 only in cells expressing PUMA$^{W\rightarrow A}$ (Fig. 4c). PUMA^{BH3} and PUMA$^{BH3\ W\rightarrow A}$ bound similarly to BCL-2-family proteins other than BCL-xL (Supplementary Fig. 15), demonstrating that the differential effects of wild-type PUMA *versus* PUMA$^{W\rightarrow A}$ were not due to differential interactions with these other BCL-2 proteins.

Discussion

Through an allosteric mechanism, PUMA binding within the hydrophobic groove uniquely distorted the BCL-xL structure near α3-α4, induced unfolding of the proximal but non-overlapping α2-α3 region, and subsequently released cytosolic p53 to engage BAX and trigger MOMP (Fig. 4d). Trp^{71} of PUMA is unique amongst BH3-only proteins and is essential for this "regulated unfolding" mechanism via a π-stacking interaction with His^{113} of BCL-xL. Substitution of Trp^{71} of PUMA with Ala supported C8-BID mediated MOMP through direct competition within the hydrophobic groove of BCL-xL but prevented p53 release and MOMP by disabling the regulated unfolding mechanism. PUMA binding-induced partial unfolding of BCL-xL increases the complexity of signaling associated with BH3 domain·BCL-xL interactions by providing two mechanisms of BAX activation: (i) derepression of C8-BID and BIM via direct competition within the hydrophobic groove[8] and (ii) allosteric control of cytosolic p53 release through regulated unfolding outside the BH3 binding groove.

Modulation of protein dynamics, including partial unfolding, through ligand binding is known to influence protein function[30–34]. In particular, enhanced dynamics over a broad range of timescales upon binding of substrates or allosteric regulators to enzymes has been associated with catalysis[30,35,36]. The role of protein dynamics in mediating molecular recognition in signaling processes has also been established[37]; however, we are unaware of examples in which regulated unfolding serves as the mechanism of signal transmission. Our data suggest that PUMA-dependent regulated unfolding of BCl-xL constitutes an unanticipated mechanism to increase signaling complexity within the apoptotic pathways. We anticipate that ligand binding-induced unfolding is a general mechanism of signal branching that may be utilized in other biological signaling pathways.

Online Methods

Reagents

Human BAD, BAK, BAX, BID, BIM, HRK, Noxa, and PUMA, and PUMA$^{W\rightarrow A}$ (>98% purity, Anaspec) and the PUMA-BAD chimeric BH3 domain peptides (>98% purity, Hartwell Center for Bioinformatics and Biotechnology, St. Jude Children's Research

Hospital) were synthesized using standard Fmoc-based chemistry with acetylation at the amino terminus and amidation at the carboxy terminus. $p53^{UVIP}$ was prepared as described[8]. The vectors for pCMVneoBam-FLAG-$PUMA^{W\rightarrow A}$, $PUMA^{W\rightarrow A}$ (pET-31, Novagen), $PUMA^{N}$ and $PUMA^{C}$ (pET-31a, Novagen) were generated using standard PCR-based cloning procedures. The His^{113} to Ala mutation was introduced in the BCL-xLΔC (pET-28, Novagen) and BCL-xLΔLΔC (pET-21, Novagen) constructs using the QuickChange site-directed mutagenesis kit (Stragene).

Protein expression

Recombinant human proteins were expressed in *E. coli* strain BL21(DE3) (Novagen). BCL-xLΔC, BCL-xLΔLΔC and full-length PUMA were expressed and purified as previously described[10]. BCL-xLΔC and BCL-xLΔLΔC are functional, recombinant forms of BCL-xL that lack the carboxy terminal 22 residues or these residues and the disordered loop between α1 and α2, respectively[18]. Recombinant human $PUMA^{W\rightarrow A}$, $PUMA^{N}$ and $PUMA^{C}$ were expressed and purified using the same procedures as for the wild type protein. Isotope labeling of the above proteins was obtained by expression in MOPS minimal media containing the appropriate labeling reagents according to established procedures[38]. Human MCL-1ΔC(in pET-151 vector, Novagen) vector was expressed as a 6X Histidine tag fusion by the addition of 1 mM IPTG. Cell pellets were resuspended in lysis buffer (50 mM Tris, pH 8.0, 500 mM NaCl, 5 mM imidazole, 5.0 mM TCEP) plus protease inhibitor mixture (Roche) and affinity purified with Ni-NTA Superflow resin (Qiagen) followed by gel filtration on a Superdex 200 preparative gel filtration column (Amersham) to >98% purity based on SDS-PAGE. Human BFL-1ΔC (in pGEX-6P3 vector, GE Healthcare) was expressed as a glutathione S-transferase (GST) tag fusion by the addition of 0.2 mM IPTG and cultured at 18 °C for 24 hr. Cell pellets were resuspended in lysis buffer (10 mM Na_2HPO_4, 2 mM KH_2PO_4, 137 mM NaCl, 2.7 mM KCl, pH 7.4) plus protease inhibitor mixture (Roche) and affinity purified with Glutathione Sepharose Fast Flow resin (GE Healthcare). The GST tag was cleaved by PreScission protease (GE Healthcare) and removed by a second GST affinity step. BFL-1ΔC was further purified by gel filtration on a Superdex 200 preparative gel filtration column (Amersham) to >98% purity based on SDS-PAGE. Human BCL-2ΔC (in pTXB1 vector, New England Biolabs) was expressed as a 6X Histidine tag fusion by the addition of 0.5 mM IPTG. Cell pellets were resuspended in lysis buffer (25 mM Tris, pH 8.0, 500 mM NaCl, 5 mM imidazole, 1 mg/mL lysozime) plus protease inhibitor mixture (Roche) and affinity purified with Ni-NTA Superflow resin (Qiagen). The protein was dialyzed against 25 mM Tris, pH 8.0, 1 mM DTT and further purified by anion exchange using a MonoQ Q-sepharose column (Amersham Biosciences). Human $p53^{SM}$ 1-360 construct, containing core stabilizing mutations[25] (in pET-28 vector, Novagen) was expressed as a 6X Histidine tag fusion by the addition of 0.5 mM IPTG. Cell pellets were resuspended in lysis buffer (25 mM Hepes, pH 7.0, 500 mM NaCl, 1 mM TCEP, 1 mg/mL lysozime) plus protease inhibitor mixture (Roche) and affinity purified with Ni-NTA Superflow resin (Qiagen). The protein was dialyzed against 25 mM bis-tris propane, pH 6.5, 50 mM NaCl, 5 mM DTT and the 6X His tag cleaved using restriction grade Thrombin (Novagen). A final heparin affinity purification step was performed (resin from GE Lifesciences). Human full length, monomeric BAX, produced as a self-cleavable chitin-binding-intein fusion from a pTYB1 vector (New England Biolabs) was purified

using the IMPACT protocol (New England Biolabs) followed by anion exchange chromatography using a MonoQ Q-sepharose column (Amersham Biosciences). All peptide and protein concentrations were determined by measurement of their optical density at 280 nm (OD_{280}) after dilution in 6 M guanidinium hydrochloride.

Circular dichroism spectropolarimetry

CD data were collected on an Aviv 62A DS spectropolarimeter. Far-UV CD wavelength scans (195–260 nm) were performed with 5 μM PUMA protein or 50 μM $PUMA^{BH3}$ in 20 mM potassium phosphate pH 7.0 using the following standard measurement parameters: wavelength, 195–260 nm; step resolution, 0.5 nm; speed, 20 nm/sec; accumulations, 10; response, 1 sec; bandwidth, 1 nm; path length, 0.1 cm. Temperature was maintained at 25 °C with a Peltier device. All CD data were converted to mean ellipticity per residue.

Calorimetric studies

ITC experiments were performed using VP-ITC or ITC200 (Microcal) calorimeters. Titrations consisted of a preliminary 2 μl injection of PUMA or indicated BH3 domain peptides, followed by several injections of 6 μl (VP-ITC) or 2 μl (ITC200) of PUMA or indicated BH3 domain peptides into a solution of BCL-xLΔC, BCL-$xLΔC^{H→A}$, BCL-xLΔLΔC, BCL-2ΔC, MCL-1ΔC, or BFL-1ΔC. The same procedure was followed for titrations of BCL-xLΔC or BCL-xLΔLΔC into a solution of $p53^{SM}$ 1-360. Unless otherwise stated, nominal sample concentrations were 10μM and 100 μM in cell and syringe respectively. Actual sample concentrations were determined after dialysis or buffer exchange by measurement of their OD_{280}. Experiments were performed at 25 °C in 20 mM Tris, pH 7.4, 100 mM NaCl and 1 mM TCEP. The time interval between injections was 300 sec. Instruments were regularly calibrated using standard procedures. Thermodynamic parameters were obtained using Origin software (OriginLab) using a 1:1 binding model with routines provided by the manufacturer. Heats of reaction were corrected for the effect of dilution.

Analytical ultracentrifugation

BCL-xLΔLΔC, BCL-xLΔLΔC ·$PUMA^{BH3}$, and 7.2, BCL-xLΔLΔC ·$PUMA^{BH3\ W→A}$, all at approximately 2 mg/ml in PBS buffer, pH were subjected to sedimentation velocity ultracentrifugation in a ProteomeLab XL-I analytical ultracentrifuge with a Beckman An-60 Ti rotor and cells containing sapphire windows and charcoal-filled Epon double-sector centerpieces (Beckman Coulter, Fullerton, CA). The density and viscosity of the buffer were calculated from their composition, and the partial specific volume and molecular weights of the protein and complexes were calculated based on their amino acid composition using the software SEDNTERP[39]. All samples were buffer exchanged against the ultracentrifugation buffer in centrifugal filter devices, and the flowthrough buffer was used as an optical reference. Temperature equilibrium at 20 °C was established in the instrument prior to the run over a period of at least 3 hr. Ultracentrifugation was performed at 60,000 rpm for 12 hr. Fringe displacement data at time intervals of 1.0 min were collected with the Rayleigh interference system and analysed with SEDFIT software using the model for continuous sedimentation coefficient distribution *c(s)* with deconvolution of diffusional effects[40,41]. The

sedimentation coefficient distribution *c(s)* was calculated with maximum entropy regularization at a confidence level of p = 0.7 and at a resolution of sedimentation coefficients of n = 120. The positions of the meniscus and bottom, as well as time-invariant and radial noises, were fitted.

Sedimentation equilibrium experiments were performed with a Beckman An-50 Ti rotor and cells containing quartz windows and charcoal-filled Epon double-sector center pieces (Beckman Coulter, Fullerton, CA). The density and viscosity of the buffer were calculated as described above. Equilibrium was attained at 24 h at a rotor temperature of 4 °C at increasing speeds of 12.8, 17.4 and 30 k rpm. Protein at concentrations 1.4 and 4.5 μM (120 μL) were loaded into double-sector centrepieces and absorbance distributions recorded at 230 and 280 nm in 0.001 cm radial intervals with 20 replicates for each point. Global least squares modelling of all datasets (all concentrations, rotor speeds and wavelengths) were performed with the software SEDPHAT using a single species model as well as a reversible monomer-dimer self-association model[42].

NMR spectroscopy

^{15}N-labeled or ^{15}N,^{13}C, ^{2}H-labeled with selective Ile, Leu, Val methyl protonation BCL-xLΔLΔC, ^{15}N,^{13}C-labeled BCL-xLΔLΔC$^{H\rightarrow A}$ and ^{15}N-labeled BCL-xLΔC proteins were prepared at the indicated concentrations in 10 mM sodium phosphate pH 7.0, 40 mM NaCl, 0.01% w/vol NaN_3, 8% $^{2}H_2O$. ^{15}N-labeled PUMA was prepared at 0.25 mM in 25 mM sodium phosphate, pH 6.8, 150 mM KCl, and 5 mM deuterated DTT (Cambridge). Data were acquired on Bruker 600 MHz and 800 MHz spectrometers equipped with cryogenically-cooled, triple-resonance single-axis gradient probes. 2D ^{1}H-^{15}N correlation spectra (using HSQC and TROSY) were acquired at 25 °C using standard Bruker pulse sequences using 16–32 scans, 2048 × 200–256 complex points, spectral windows of 14 × 32 ppm in the ^{1}H and ^{15}N dimensions, respectively. {^{1}H}-^{15}N heteronuclear NOE experiments were collected at 25 °C using 24–40 scans, 2048 × 300 complex points using similar spectral windows as above. The recycle delay was 1 s for HSQC and TROSY experiments and 4 s for heteronuclear NOE experiments. The following 3D experiments were performed using 0.9 mM samples of either free BCL-xLΔLΔC or BCL-xLΔLΔC·PUMA^{BH3} complex (in ^{15}N,^{13}C, ^{2}H, ^{1}H - Ile, Leu,Val - methyl labeled form) for resonance assignment and structure calculation: HNCA, HN(CO)CA (free BCL-xLΔLΔC only), HNCACB, CBCA(CO)NH (free BCL-xLΔLΔC only), HNCO, HN(CA)CO for backbone assignment; HCC-TOCSY for Ile, Leu, Val side-chain methyl assignment; and ^{13}C-edited aliphatic HSQC-NOESY and ^{15}N-edited TROSY-NOESY for Ile, Leu, Val methyl assignment and distance restraints. A HNCA spectrum was collected for a 0.2 mM BCL-xLΔLΔC$^{H\rightarrow A}$·PUMA^{BH3} sample to confirm the assignments of resonances most perturbed by the introduction of the mutation. 3D experiments were collected using 8–32 scans (depending on experiment sensitivity), over 2048 × 40–64 × 80–128 complex points and processed with linear prediction and zero filling in the indirect dimensions with spectral windows of 14 ppm (^{1}H), 30 ppm (^{15}N), 18 ppm (^{13}C HNCO, HN(CA)CO), 32 ppm (^{13}C, HNCA, HN(CO)CA), 70 ppm, (^{13}C, HNCACB), and 70 ppm (^{13}C, HCC-TOCSY) with appropriate offsets. A NOE mixing time of 120 ms was employed. For resonance assignments of the unlabeled PUMA^{BH3} peptide in complex with labeled BCL-xL, ^{15}N-filtered 2D NOESY and TOCSY

spectra were collected over 128 or 48 scans respectively, 2048 × 512 complex points and spectral windows of 12 ppm in both F2 and F1 dimensions. Spectra were processed using NMRPipe[43] or TopSpin (Bruker Biospin) and analyzed with CARA[44] software. Assignments for the BCL-xLΔC construct were kindly provided by Dr. Philipp Selenko (FMP, Berlin).

Comment on solution structure determination strategy

The solution structure of the BCL-xLΔLΔC·PUMA^{BH3} complex was determined by NMR methods exploiting selective isotope labeling of BCL-xLΔLΔC. Protonated methyl moieties of Ile, Leu, Val side-chains were introduced within an otherwise fully ^{15}N,^{13}C,^{2}H-labeled polypeptide backbone[45–47]. This labeling scheme generates a limited number of NOE cross-peaks, which simplifies the interpretation and assignment of NOESY datasets, but also provides sufficient restraints for accurate structure determination[48]. In particular it allowed the unambiguous assignment of inter-molecular cross peaks between isotope-labeled BCL-xLΔLΔC and protonated side-chains of the PUMA^{BH3} peptide. A potential limitation of this strategy, however, is insufficient sampling of distance restraints. Under-sampling of restraints would produce under-determined structural models with poor convergence. To address this concern, we determined the structure of apo BCL-xLΔLΔC using the same strategy as for the BCL-xLΔLΔC·PUMA^{BH3} complex (Supplementary. Table 1). The 20 lowest energy structures for BCL-xLΔLΔC exhibited Cα and heavy atom r.m.s.d. values of 1.01±0.26 Å and 1.71±0.28 Å respectively for the folded core of the protein. These r.m.s.d. values are only marginally larger than those reported for the solution structure of fully protonated BCL-xLΔC (PDB: 1LXL; Cα r.m.s.d., 0.54±0.10 Å; heavy atom r.m.s.d., 1.03±0.12 Å; Supplementary. Fig. 16). The ensemble of 20 lowest energy structures displayed backbone r.m.s.d. of 2.06 Å from the x-ray structure of BCL-xLΔC (PDB: 1R2D, Supplementary. Fig 16 c). Therefore, due to the accuracy of apo BCL-xLΔLΔC relative to published findings, the sparse methyl protonation labeling strategy was used to determine the structure of the BCL-xLΔLΔC·PUMA^{BH3} complex in solution.

Solution structure calculations

Structure calculations of apo BCL-xLΔLΔC and BCL-xLΔLΔC·PUMA^{BH3} complex were performed using the program Cyana[49]. Simulated annealing in torsion angle space was performed for each run on 100 structures with the 20 models scoring the lowest target function representing the final NMR structures. Distance restraints were generated from volumes of NOESY cross-peaks (integrated with CARA) using the Cyana CALIBA tool. Manual corrections were applied to the calibrations in cases of obvious peak overlap. Dihedral restraints were generated from available backbone and side-chain Cβ assignments using the program TALOS[50]. Helical hydrogen bond restraints (i to i-4) were applied between residues that showed lack of water exchange peaks in 3D NOESY spectra in combination with α-helical backbone torsion angle restraints (for a summary of restraints involving the PUMA^{BH3} peptide refer to Supplementary Fig. 17). Calculations were performed iteratively with correction of restraints calibration (and occasionally assignment) until no significant improvement of the target function could be attained. Structures were energy minimized using the Amber force field implemented in the UCSF Chimera software suite[51]. The program ProCheck[52] within the SWISS-MODEL Structure Assessment tool[53]

was used to analyze the quality of the models. The Ramachandran statistics for the two models were as follows. For BCL-xLΔLΔC: 78.3% of all residues (and 94.4% of residues within well restrained portions of the protein) were in favored regions of the Ramachandran plot, 20.7% (5.6%) in allowed regions, and 1.0% (0.0) in disallowed regions. For BCL-xLΔLΔC·PUMA^{BH3}: 72.5% (93.1%) of residues were favored; 25.8% (6.8%) allowed, and 1.7% (0.1%) disallowed.

Crystallization, data collection and refinement

The BCL-xLΔC ·PUMA^{BH3} complex was prepared by adding PUMA^{BH3} in a 1:1.2 molar ratio to 1.5 mM BCL-xLΔC in 50 mM Tris, 100 mM NaCl pH 7.5. Crystals were grown at 18°C by hanging-drop vapor diffusion mixing equal volumes of protein solution and precipitant (0.2 M calcium chloride, 0.1 M sodium acetate pH 4.6 and 20% isopropanol). The final pH of the drop was approximately 7.2. Crystals were cryoprotected in mother liquor supplemented with 30% glycerol and flash-frozen in liquid nitrogen. Diffraction data were collected at 100 K at the Southeast Regional Collaborative Access Team (SER-CAT) 22-ID synchrotron beamline using a CCD detector and a beam wavelength of 1.0 Å. Data were indexed and scaled using HKL2000[54]. The structure of the BCL-xLΔC·PUMA^{BH3} complex was determined by molecular replacement using PHASER[55]. Model building was performed using COOT[56], and iterative rounds of refinement were performed using PHENIX[57]. The asymmetric unit contained two BCL-xLΔC monomers, molecules ‘A’ and ‘B’, each of which created domain-swapped dimers around 2-fold axes. Molecule A was well resolved due to its superior electron density. Electron density for PUMA^{BH3} was clearly visible in proximity of molecule A, but weak and poorly defined near molecule B. The PUMA^{BH3} peptide was therefore modeled and refined in complex with molecule A only. The Ramachandran statistics for the model were as follows: 95.4% of residues in favored regions, 4.6% in allowed regions, 0.0% in disallowed regions. All structural Figures were generated with PyMOL (www.pymol.org) or the UCSF Chimera package[51].

Fluorescence polarization

A BCL-xLΔC C151S/S2C double mutant was generated with the QuickChange site-directed mutagenesis kit (Stratagene). The protein was labeled with 5-Iodoacetamidofluorescein (5-IAF, Thermo Scientific) in its stock buffer (25 mM Tris, 200 mM NaCl, 1 mM EDTA, 5 mM DTT, pH 7.5) according to the manufacturer’s reaction protocol in presence of DTT. Excess unreacted dye was removed by extensive buffer exchange over a centrifugal device. The fluorescently labeled product, F- BCL-xLΔC, was used at 100 nM in all experiments. Fluorescence polarization measurements were performed at 25 °C in 96-well plates on a Perkin Elmer EnVision plate reader equipped with FITC excitation and emission filters. Instrument settings were optimized automatically. Experiments were performed at 25±2 °C in 10 mM phosphate, 40 mM NaCl, 5 mM DTT, pH 7.0. All experiments were performed with 3–5 replicates. Polarization values were calibrated against samples of fluorescein solution. Direct binding titrations were fit to a Langmuir Isotherm equation. Binding competition titrations were fit to the following quadratic equation, derived from thermodynamic consideration upon the approximation that the concentration of the fluorescent probe must be significantly smaller than that of the other species:

$$FP^{obs}=FP^{0}+\Delta FP \cdot \frac{-[K_{comp}\cdot(X-p53)+2\cdot p53+K_D^{FBCLxL}]+\sqrt{[K_{comp}\cdot(X-p53)+2\cdot p53+K_D^{FBCLxL}]^2+4\cdot p53\cdot[K_{comp}\cdot(X-p53)+K_{c}}}{2\cdot[K_{comp}\cdot(X-p53)+K_{comp}\cdot K_D^{FBCLxL}-p53-K_D^{FBCLxL}]}$$

where FP^0 and ΔFP are scaling factor to fit the 0 to 1 range of the equation to fluorescence polarization endpoint values; $K_{comp} = K_D^{FBCLxL}/K_D^{app}$; K_D^{FBCLxL} is the dissociation constant between F-BCL-xLΔC and $p53^{SM}$ 1-360; K_D^{app} is the apparent dissociation constant between the competing, non-fluorescent species (i.e. BCL-xLΔC, BCL-xLΔC$^{H\rightarrow A}$ or BCL-xLΔC$^{H\rightarrow A}$ ·PUMA^{BH3}) and $p53^{SM}$ 1-360; p53 is the concentration of $p53^{SM}$ 1-360; X is the variable concentration of competing, non-fluorescent species. The fitted parameters were FP^0, Δ^{FP} and K_{comp}. Curve fitting was performed using KaleidaGraph software.

Electrophoresis, immunoblotting and co-immunoprecipitation

SDS-PAGE was conducted using the Criterion XT 4–12% gel system (BioRad) with 1X MOPS buffer at 150 V. Native PAGE was performed on 18% Tris-HCl polyacrylamide gels (BioRad) in native running buffer (25 mM Tris pH 8.3, 192 mM glycine), and samples were prepared using the Native PAGE Sample Loading Kit (Invitrogen). For western blot analysis, proteins were transferred to nitrocellulose by standard conditions, blocked in 5% milk/Tris Buffered Saline Tween-20 (TBST) and primary antibodies (in blocking buffer): BCL-xL (SantaCruz Biotechnology, clone S-18) 1:1,000; cytochrome c (Pharmingen, clone 7H8.2C12) 1:1,000; p53 (SantaCruz Biotechnology, clone D07) 1:1,000; PUMA (Cell Signaling or Sigma) 1:1,000 and FLAG (SantaCruz Biotechnology, clone M2) 1:1,000 were incubated overnight at 4 °C. The secondary antibody (1:5,000 in blocking buffer) was incubated at 25 °C for 1 hr before standard enhanced chemiluminescence detection.

BCL-xLΔC·p53 complexes were produced for co-immunoprecipitation by combining 10 nM recombinant BCL-xLΔC with $p53^{UVIP}$ in HE buffer (10 mM HEPES, pH 7.4, 1 mM EDTA) overnight at 4 °C[2,8]. Anti-BCL-xL (clone H-5) or anti-p53 (clone DO7) antibodies and protein A/G-agarose beads (Thermo Scientific) were added, incubated overnight at 4 °C, and washed 3 times to remove any unbound material. Protein A/G-agarose beads were boiled in 1X SDS-PAGE loading dye, and precipitated proteins were visualized by standard SDS-PAGE and western blot techniques.

For FLAG-PUMA co-immunoprecipitations, cells were lysed in 1% CHAPS, 150 mM NaCl, 5 mM $MgCl_2$, 1 mM EDTA and 10% glycerol. Lysates (100 mg) were combined with 1 mg FLAG M2 antibody, 25 ml 50% slurry of Protein A/G Plus Agarose (Santa Cruz Biotechnology) and incubated end over end for 2 hours at 4°C. Agarose beads were washed 3 times in lysis buffer, eluted with 100 μg/ml FLAG peptide, and precipitated proteins were visualized by standard SDS-PAGE and western blot techniques.

For BCL-xL immunoprecipitations and assessment of its oligomeric state in association with PUMA, MCF7 cells stably expressing HA-tagged BCL-xL were UV treated (100 mJ/cm^2) and cells lysed six hours after irradiation in 2% CHAPS, 300 mM NaCl, 25 mM Tris pH 7.6 and 1 mM DTT. Lysates were combined with monoclonal anti-HA-Agarose beads (Sigma)

overnight at 4 °C. Agarose beads were washed three times in lysis buffer, eluted with 100 μg/ml HA peptide, and precipitated proteins were visualized by standard SDS PAGE AND Native PAGE followed by western analysis of HA-BCL-xL (using an HA antibody from Sigma).

Heavy membrane preparation and cytochrome c release

Heavy membrane fractions (referred to as mitochondria) were purified from murine liver, usually female, under 3 months, using dounce homogenization and differential centrifugation in mitochondrial isolation buffer (MIB: 200 mM mannitol, 68 mM sucrose, 10 mM HEPES-KOH pH 7.4, 10 mM KCl, 1 mM EDTA, 1 mM EGTA, 0.1 % BSA). For MOMP assays, mitochondria were incubated in MIB supplemented to 110 mM KCl (mitochondrial assay buffer, MAB), plus or minus proteins and peptides (final concentrations and order of addition are indicated in the text and figure legends) for 60 minutes at 37 °C. Reactions were then fractionated into supernatant and pellet by centrifugation at 5,500 × g for 5 min, and analyzed by SDS-PAGE and western blot with an anti-cytochrome c antibody. For MOMP reconstitution studies, heavy membrane fractions were isolated from the livers of poly-dIdC-treated *MxCre* $bak^{-/-}bax^{f/-}$ animals (referred to as $bak^{-/-}bax^{-/-}$), which removed the remaining *bax* allele. Human, full-length, monomeric BAX promoted complete cytochrome c release at 20 nM. For concurrent binding and MOMP assays, 10 nM BCL-xLΔC·$p53^{UVIP}$ complexes were produced and captured by combining recombinant BCL-xLΔC, $p53^{UVIP}$ and Ni^{+2}-NTA agarose in PBS at 25 °C for 2 hrs before pelleting (1,000 × g, 5 minutes at 25 °C) and washing the complex three times with PBS. The final pellet was resuspended in MAB (without EDTA or EGTA), indicated peptides were added along with BAX and mitochondria, and incubated for 1 hr at 37 °C before fractionation and western blot analysis for cytochrome c, BCL-xLΔC and $p53^{UVIP}$.

Cell culture, transfection and survival assays

Mouse embryonic fibroblasts (MEFs; SV40 immortalized wild type, $p53^{-/-}$ and $puma^{-/-}$) were cultured in DMEM containing 10% FBS, 100 mM 2-mercaptoethanol, 2 mM L-glutamine and antibiotics. The MEF panel was routinely replaced to minimize culture-induced accumulation of direct activator proteins. Cells were transfected using Lipofectamine 2000 according to the manufacturer's instructions for 6 hours under serum-free conditions (pCMV5 and pCMVneoBam-FLAG-PUMA wild type or W71A). Green fluorescent protein (pUS9-GFP) was co-transfected as an efficiency marker (30–50% of cells were usually transfected). The next day, cells were treated with indicated doses of TNF/CHX or UV for 6 h and 24 h, respectively; before trypsinization, RIPA lysis, immunoprecipitation and/or AnnexinV-PE labeling and analysis by flow cytometry.

Database Depositions

The atomic coordinates (or 20 lowest-energy structures) and structure factors (or NMR assignments) for the X-ray-derived (NMR-derived) models described in this manuscript have been deposited in the PDB (NMR assignments deposited in the BioMAgRes Databank): solution structure of apo BCL-xLΔLΔC: 2M03 (BMRB #18792); solution structure of monomeric, 1:1 BCL-xLΔLΔC·$PUMA^{BH3}$ complex: 2M04 (BMRB #18793);

and X-ray structure of domain-swapped, 2:2 dimeric BCL-xLΔC·PUMA^{BH3} complex: 4HNJ.

Supplementary Material

Refer to Web version on PubMed Central for supplementary material.

Acknowledgments

We thank Drs. Joseph T. Opferman and Stephen W. G. Tait (St. Jude Children's Research Hospital) for the *MxCre bak*$^{-/-}$*bax*$^{f/-}$ animals and MCF7 SMAC-GFP cells, respectively. The prokaryotic expression vectors for PUMAβ and BCL-xLΔLΔC were kindly provided by Dr. Eric Eldering (Academic Medical Center, Amsterdam) and Gerhard Wagner (Harvard University), respectively. We would like to acknowledge Dr. Darcie Miller (St. Jude Children's Research Hospital) for help with synchrotron data collection. SER-CAT supporting institutions may be found at www.ser.anl.gov/new/index.html. Use of the SER-CAT Advanced Photon Source was supported by the U. S. Department of Energy, Office of Science, Office of Basic Energy Sciences, under Contract No. W-31-109-Eng-38. We would like to thank Bruker BioSpin and Drs. Rüdiger Weismann and Wolfgang Bermel for access to a 950 MHz NMR spectrometer. We also thank Dr. M. Madan Babu and A. Venkatakrishnan (MRC Laboratory of Molecular Biology, Cambridge, UK) for stimulating discussions and comments on the manuscript. This work was supported by NIH R01CA082491 and 1R01GM083159 (to R.W.K), NIH R01GM52735 and R01GM96208 (to D.R.G), NIH R01 CA157740 (to J.E.C), the JJR Foundation (to J.E.C.), the William A. Spivak Fund (to J.E.C.), the Fridolin Charitable Trust (to J.E.C.), an NCI Cancer Center Support Grant P30CA21765 (at St. Jude Children's Research Hospital), Research Grant No. 5-FY11-74 from the March of Dimes Foundation (to J.E.C.), and the American Lebanese Syrian Associated Charities (ALSAC). J.C.F. is a recipient of the Alma and Hal Reagan Cancer Research fellowship provided by the University of Tennessee Health Sciences Center.

References and Notes

1. Green DR, Kroemer G. Cytoplasmic functions of the tumour suppressor p53. Nature. 2009; 458:1127–1130. [PubMed: 19407794]
2. Chipuk JE, Bouchier-Hayes L, Kuwana T, Newmeyer DD, Green DR. PUMA couples the nuclear and cytoplasmic proapoptotic function of p53. Science. 2005; 309:1732–1735. [PubMed: 16151013]
3. Nakano K, Vousden KH. PUMA, a novel proapoptotic gene, is induced by p53. Mol Cell. 2001; 7:683–694. [PubMed: 11463392]
4. Yu J, Zhang L, Hwang PM, Kinzler KW, Vogelstein B. PUMA induces the rapid apoptosis of colorectal cancer cells. Mol Cell. 2001; 7:673–682. [PubMed: 11463391]
5. Jeffers JR, et al. Puma is an essential mediator of p53-dependent and -independent apoptotic pathways. Cancer Cell. 2003; 4:321–328. [PubMed: 14585359]
6. Chen L, et al. Differential targeting of prosurvival Bcl-2 proteins by their BH3-only ligands allows complementary apoptotic function. Mol Cell. 2005; 17:393–403. [PubMed: 15694340]
7. Kuwana T, et al. BH3 domains of BH3-only proteins differentially regulate Bax-mediated mitochondrial membrane permeabilization both directly and indirectly. Mol Cell. 2005; 17:525–535. [PubMed: 15721256]
8. Chipuk JE, et al. Direct activation of Bax by p53 mediates mitochondrial membrane permeabilization and apoptosis. Science. 2004; 303:1010–1014. [PubMed: 14963330]
9. Leu JI, Dumont P, Hafey M, Murphy ME, George DL. Mitochondrial p53 activates Bak and causes disruption of a Bak-Mcl1 complex. Nat Cell Biol. 2004; 6:443–450. [PubMed: 15077116]
10. Chipuk JE, et al. Mechanism of apoptosis induction by inhibition of the anti-apoptotic BCL-2 proteins. Proc Natl Acad Sci U S A. 2008; 105:20327–20332. [PubMed: 19074266]
11. Hinds MG, et al. Bim, Bad and Bmf: intrinsically unstructured BH3-only proteins that undergo a localized conformational change upon binding to prosurvival Bcl-2 targets. Cell Death Differ. 2007; 14:128–136. [PubMed: 16645638]
12. Sattler M, et al. Structure of Bcl-xL-Bak peptide complex: recognition between regulators of apoptosis. Science. 1997; 275:983–986. [PubMed: 9020082]

13. Petros AM, et al. Rationale for Bcl-xL/Bad peptide complex formation from structure, mutagenesis, and biophysical studies. Protein Sci. 2000; 9:2528–2534. [PubMed: 11206074]
14. Feng W, Huang S, Wu H, Zhang M. Molecular basis of Bcl-xL's target recognition versatility revealed by the structure of Bcl-xL in complex with the BH3 domain of Beclin-1. J Mol Biol. 2007; 372:223–235. [PubMed: 17659302]
15. Liu X, Dai S, Zhu Y, Marrack P, Kappler JW. The structure of a Bcl-xL/Bim fragment complex: implications for Bim function. Immunity. 2003; 19:341–352. [PubMed: 14499110]
16. Petros AM, Gunasekera A, Xu N, Olejniczak ET, Fesik SW. Defining the p53 DNA-binding domain/Bcl-x(L)-binding interface using NMR. FEBS Lett. 2004; 559:171–174. [PubMed: 14960327]
17. Hagn F, et al. BclxL changes conformation upon binding to wild-type but not mutant p53 DNA binding domain. J Biol Chem. 2010; 285:3439–3450. [PubMed: 19955567]
18. Muchmore SW, et al. X-ray and NMR structure of human Bcl-xL, an inhibitor of programmed cell death. Nature. 1996; 381:335–341. [PubMed: 8692274]
19. Berjanskii M, Wishart DS. NMR: prediction of protein flexibility. Nat Protoc. 2006; 1:683–688. [PubMed: 17406296]
20. O'Neill JW, Manion MK, Maguire B, Hockenbery DM. BCL-XL dimerization by three-dimensional domain swapping. J Mol Biol. 2006; 356:367–381. [PubMed: 16368107]
21. Denisov AY, Sprules T, Fraser J, Kozlov G, Gehring K. Heat-induced dimerization of BCL-xL through alpha-helix swapping. Biochemistry. 2007; 46:734–740. [PubMed: 17223694]
22. Day CL, et al. Structure of the BH3 domains from the p53-inducible BH3-only proteins Noxa and Puma in complex with Mcl-1. J Mol Biol. 2008; 380:958–971. [PubMed: 18589438]
23. Smits C, Czabotar PE, Hinds MG, Day CL. Structural plasticity underpins promiscuous binding of the prosurvival protein A1. Structure. 2008; 16:818–829. [PubMed: 18462686]
24. Nikolova PV, Henckel J, Lane DP, Fersht AR. Semirational design of active tumor suppressor p53 DNA binding domain with enhanced stability. Proc Natl Acad Sci U S A. 1998; 95:14675–14680. [PubMed: 9843948]
25. Joerger AC, Allen MD, Fersht AR. Crystal structure of a superstable mutant of human p53 core domain. Insights into the mechanism of rescuing oncogenic mutations. J Biol Chem. 2004; 279:1291–1296. [PubMed: 14534297]
26. Xu HB, et al. The MDM2-Binding Region in the Transactivation Domain of p53 Also Acts as a Bcl-X-L-Binding Motif. Biochemistry. 2009; 48:12159–12168. [PubMed: 19916559]
27. Letai A, et al. Distinct BH3 domains either sensitize or activate mitochondrial apoptosis, serving as prototype cancer therapeutics. Cancer Cell. 2002; 2:183–192. [PubMed: 12242151]
28. Kim H, et al. Stepwise activation of BAX and BAK by tBID, BIM, and PUMA initiates mitochondrial apoptosis. Mol Cell. 2009; 36:487–499. [PubMed: 19917256]
29. Ren D, et al. BID, BIM, and PUMA are essential for activation of the BAX- and BAK-dependent cell death program. Science. 2010; 330:1390–1393. [PubMed: 21127253]
30. Miyashita O, Onuchic JN, Wolynes PG. Nonlinear elasticity, proteinquakes, and the energy landscapes of functional transitions in proteins. Proc Natl Acad Sci U S A. 2003; 100:12570–12575. [PubMed: 14566052]
31. Swain JF, Gierasch LM. The changing landscape of protein allostery. Curr Opin Struct Biol. 2006; 16:102–108. [PubMed: 16423525]
32. Frederick KK, Marlow MS, Valentine KG, Wand AJ. Conformational entropy in molecular recognition by proteins. Nature. 2007; 448:325–329. [PubMed: 17637663]
33. Henzler-Wildman K, Kern D. Dynamic personalities of proteins. Nature. 2007; 450:964–972. [PubMed: 18075575]
34. Tzeng SR, Kalodimos CG. Dynamic activation of an allosteric regulatory protein. Nature. 2009; 462:368–372. [PubMed: 19924217]
35. Boehr DD, McElheny D, Dyson HJ, Wright PE. The dynamic energy landscape of dihydrofolate reductase catalysis. Science. 2006; 313:1638–1642. [PubMed: 16973882]

36. Masterson LR, et al. Dynamically committed, uncommitted, and quenched states encoded in protein kinase A revealed by NMR spectroscopy. Proc Natl Acad Sci U S A. 2011; 108:6969–6974. [PubMed: 21471451]
37. Smock RG, Gierasch LM. Sending signals dynamically. Science. 2009; 324:198–203. [PubMed: 19359576]
38. Wang Y, Filippov I, Richter C, Luo R, Kriwacki RW. Solution NMR studies of an intrinsically unstructured protein within a dilute, 75 kDa eukaryotic protein assembly; probing the practical limits for efficiently assigning polypeptide backbone resonances. Chembiochem. 2005; 6:2242–2246. [PubMed: 16270364]
39. Laue, TM.; Shah, BD.; Ridgeway, TM.; Pelletier, SL. The Royal Society of Chemistry. Harding, SE.; Rowe, AJ.; Horton, JC., editors. 1992. p. 90-125.
40. Schuck P. Size-distribution analysis of macromolecules by sedimentation velocity ultracentrifugation and lamm equation modeling. Biophys J. 2000; 78:1606–1619. [PubMed: 10692345]
41. Schuck P, Perugini MA, Gonzales NR, Howlett GJ, Schubert D. Size-distribution analysis of proteins by analytical ultracentrifugation: strategies and application to model systems. Biophys J. 2002; 82:1096–1111. [PubMed: 11806949]
42. Balbo A, Brown PH, Braswell EH, Schuck P. Measuring protein-protein interactions by equilibrium sedimentation. Curr Protoc Immunol. 2007; Chapter 18(Unit 18):18.
43. Delaglio F, et al. NMRPipe: a multidimensional spectral processing system based on UNIX pipes. J Biomol NMR. 1995; 6:277–293. [PubMed: 8520220]
44. Keller, RJJ. Optimizing the process of nuclear magnetic resonance spectrum analysis and computer aided resonance assignment. Eidgenossische Technishe Hochschule; 2005.
45. Religa TL, Ruschak AM, Rosenzweig R, Kay LE. Site-directed methyl group labeling as an NMR probe of structure and dynamics in supramolecular protein systems: applications to the proteasome and to the ClpP protease. J Am Chem Soc. 2011; 133:9063–9068. [PubMed: 21557628]
46. Tugarinov V, Kay LE. Ile, Leu, and Val methyl assignments of the 723-residue malate synthase G using a new labeling strategy and novel NMR methods. J Am Chem Soc. 2003; 125:13868–13878. [PubMed: 14599227]
47. Tugarinov V, Kay LE. An isotope labeling strategy for methyl TROSY spectroscopy. J Biomol NMR. 2004; 28:165–172. [PubMed: 14755160]
48. Tugarinov V, Choy WY, Orekhov VY, Kay LE. Solution NMR-derived global fold of a monomeric 82-kDa enzyme. Proc Natl Acad Sci U S A. 2005; 102:622–627. [PubMed: 15637152]
49. Guntert P. Automated NMR structure calculation with CYANA. Methods Mol Biol. 2004; 278:353–378. [PubMed: 15318003]
50. Cornilescu G, Delaglio F, Bax A. Protein backbone angle restraints from searching a database for chemical shift and sequence homology. Journal of Biomolecular Nmr. 1999; 13:289–302. [PubMed: 10212987]
51. Pettersen EF, et al. UCSF Chimera - a visualization system for exploratory research and analysis. J Comput Chem. 2004; 25:1605–1612. [PubMed: 15264254]
52. Laskowski RA, Rullmannn JA, MacArthur MW, Kaptein R, Thornton JM. AQUA and PROCHECK-NMR: programs for checking the quality of protein structures solved by NMR. Journal of Biomolecular Nmr. 1996; 8:477–486. [PubMed: 9008363]
53. Kiefer F, Arnold K, Kunzli M, Bordoli L, Schwede T. The SWISS-MODEL Repository and associated resources. Nucleic Acids Res. 2009; 37:D387–392. [PubMed: 18931379]
54. Otwinowski Z, Minor W. Processing of X-ray Diffraction Data Collected in Oscillation Mode. Meth Enzymol. 1997; 276:307–326.
55. Zwart PH, et al. Automated structure solution with the PHENIX suite. Methods Mol Biol. 2008; 426:419–435. [PubMed: 18542881]
56. Emsley P, Cowtan K. Coot: model-building tools for molecular graphics. Acta Crystallogr D Biol Crystallogr. 2004; 60:2126–2132. [PubMed: 15572765]
57. Adams PD, et al. PHENIX: a comprehensive Python-based system for macromolecular structure solution. Acta Crystallogr D Biol Crystallogr. 2010; 66:213–221. [PubMed: 20124702]

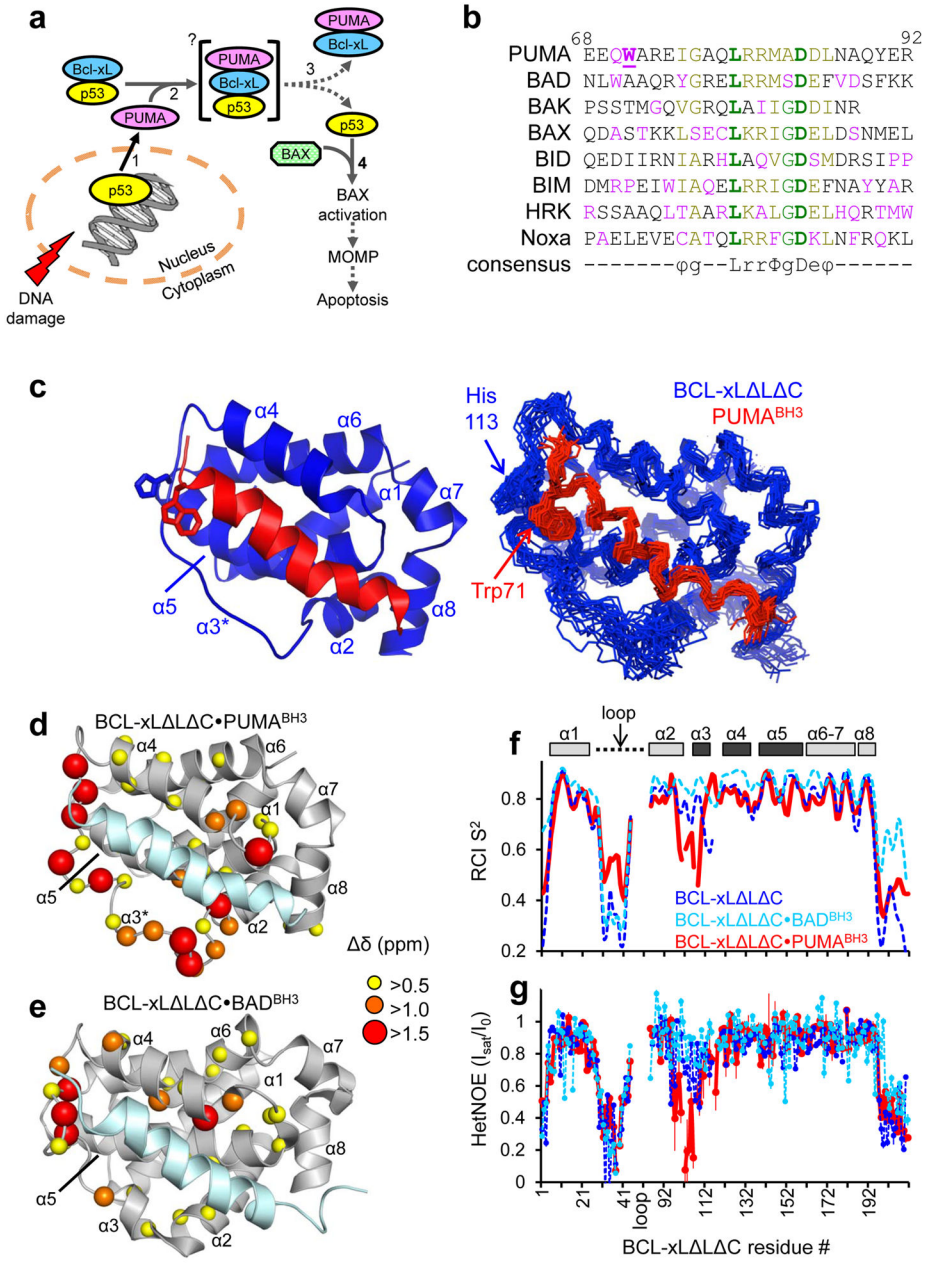

Figure 1.

Structural and dynamic characterization of the BCL-xLΔLΔC·PUMA^{BH3} complex in solution. **a**. Scheme illustrating the mechanism by which p53 regulates apoptosis through interactions with DNA in the nucleus and BCL-2 family proteins in the cytosol. Increasing numerals denote the sequence of events involved in this process. **b**. Sequence alignment of BH3 domains, color-coded according to conservation (bold green: conserved; green: highly conserved; olive: partially conserved; red: unique). The consensus motif is indicated: φ hydrophobic residue; g Gly, Ser or Ala; L Leu; r usually Arg or Lys; Φ hydrophobic residue; D Asp; and e usually Glu or Asp. Unique residues in the PUMA BH3 domain are Gln^{70} and Trp^{71}; residue numbers for PUMA are given at the top. These sequences correspond to the

synthetic peptides employed in this study. **c**. Solution structure of the BCL-xLΔLΔC·PUMA^{BH3} complex; ribbon representation of the lowest-energy structure (left) and alignment of the 20 lowest-energy structures (right). BCL-xLΔLΔC is colored blue and PUMA^{BH3} is colored red. **d**. Structural representation of ^{1}H-^{15}N NMR chemical shift perturbations caused by PUMA^{BH3} binding to BCL-xLΔLΔC. **e**. Equivalent representations for the BCL-xLΔLΔC·BAD^{BH3} complex (PDB: 1G5J; BMRB entry: 6578)[13]. **f**. Sequence dependence of random coil index order parameter (RCI S^2) for free BCL-xLΔLΔC (blue), BCL-xLΔLΔC·BAD^{BH3} (light blue), and BCL-xLΔLΔC·PUMA^{BH3} (red). The BH3 interaction site is highlighted above the graph (dark gray) within a schematic representation of the protein's α-helices. **g**. Sequence dependence of {^{1}H}-^{15}N HetNOE values for the same proteins as illustrated in **f**. Error bars are inversely proportional to the signal-to-noise ratio of each resonance.

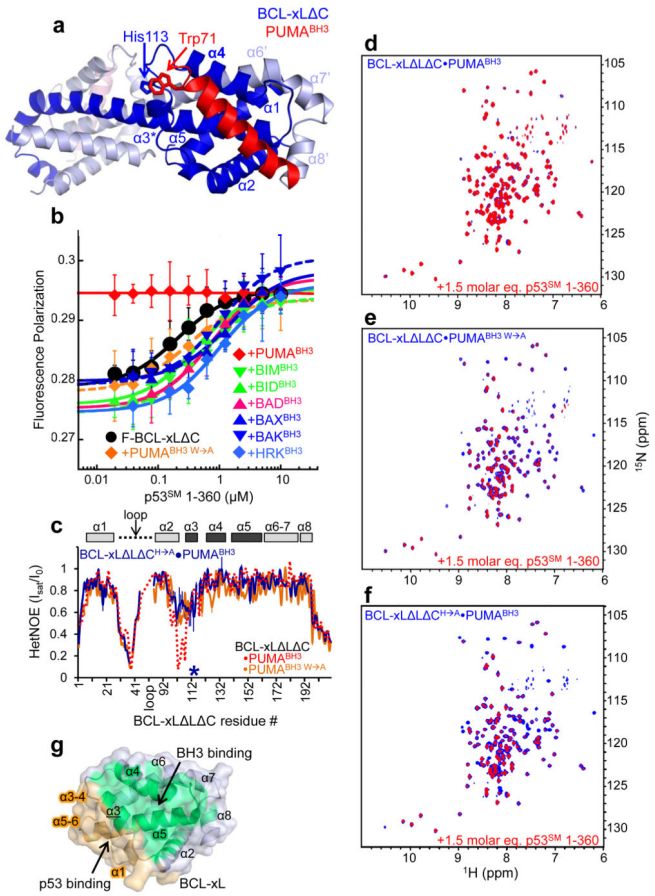

Figure 2.

Mechanism of PUMA binding-induced p53 release from BCL-xL. **a**. Crystal structure of BCL-xLΔC domain-swapped dimer bound to PUMA^{BH3}. The two subunits of BCL-xLΔC are colored dark blue and light blue, respectively, and the eight α-helices of one globular core of the dimer (right side) are labeled α1-α5 and α6′-α8′. The two molecules of PUMA^{BH3} are colored red (front, right) and light red (back, left), respectively. The imidazole ring of His^{113} of BCL-xL and the indole ring of Trp^{71} of PUMA^{BH3} that are engaged in a π-stacking interaction are indicated. **b**. Fluorescence polarization analysis of titrations of p53^{SM} 1-360 into fluorescently labeled BCL-xLΔC (F-BCL-xLΔC), isolated or previously bound to a slight molar excess of different BH3 peptides from PUMA, BIM, BID, BAD, BAX, BAK or HRK as indicated. Error bars represent the standard error of the mean of five independent titrations. **c**. Sequence dependence of {^{1}H}-^{15}N HetNOE values for BCL-xLΔLΔC in complex with PUMA$^{BH3\ W\rightarrow A}$ (orange) and BCL-xLΔLΔC$^{H\rightarrow A}$ in complex with wild-type PUMA^{BH3} (blue; the mutation site is marked with an asterisk). The values observed for BCL-xLΔLΔC·PUMA^{BH3} (Fig. 1g) are illustrated with a dashed red line. **d–f**. Overlaid 2D ^{1}H-^{15}N TROSY spectra of 100 μM ^{15}N-BCL-xLΔLΔC bound to unlabeled PUMA^{BH3} (**d**), PUMA$^{BH3\ W\rightarrow A}$ (**e**) or ^{15}N-BCL-xLΔLΔC$^{H\rightarrow A}$ bound to PUMA^{BH3} (**f**) in the absence (blue) and presence (red) of a 1.5 molar excess of p53^{SM} 1-360. **g**. Surface representation of apo BCL-xL highlighting the non-overlapping nature of its surfaces that bind to BH3 domains, including PUMA^{BH3} (green) and p53 (orange).

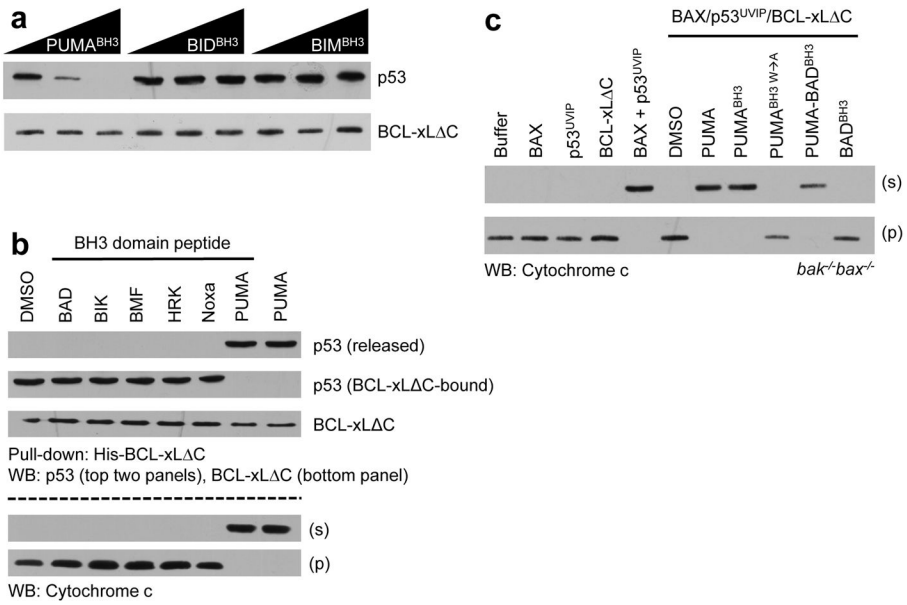

Figure 3.

PUMA-induced p53 release from BCL-xL differentially regulates apoptotic pathways. **a**. His-tagged BCL-xLΔC·p53^{UVIP} complexes were combined with PUMA^{BH3} or the indicated direct activator BH3 domain peptides (10, 50 and 100 nM concentrations); His-BCL-xLΔC was then isolated using nickel affinity beads. His-BCL-xLΔC and associated p53 were detected after SDS-PAGE by western blot analyses. **b**. His-BCL-xLΔC·p53^{UVIP} complexes (20 nM) were combined with *bak*$^{-/-}$*bax*$^{-/-}$ mitochondria in the presence of BAX and indicated derepressor BH3 domain peptides or PUMA (40 nM), followed by fractionation and either nickel affinity pull-down of His-BCL-xLΔC, SDS-PAGE and western blot analyses for p53 and BCL-xL (upper panels), or western blot analysis for mitochondrial (labeled “p”) or released (labeled “s”) cytochrome c (lower panels). **c**. BCL-xLΔC·p53^{UVIP} complexes (the two components were mixed at 100 nM and 10 nM concentrations respectively) were combined with *bak*$^{-/-}$*bax*$^{-/-}$ liver mitochondria in the presence of BAX (20 nM) and the indicated derepressor BH3 domain peptides (1 μM) or PUMA (100 nM) before fractionation, SDS-PAGE and western blot analyses for cytochrome c.

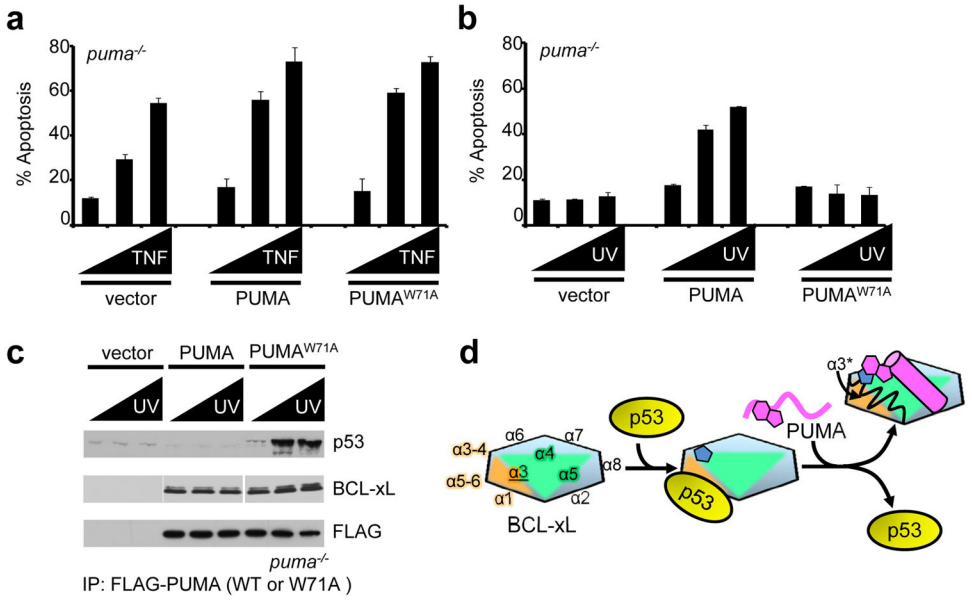

Figure 4.

Trp^{71} (W71) of PUMA is required for p53-dependent, DNA damage-induced apoptosis. **a**. *puma*$^{-/-}$ MEFs were transiently transfected with pCMVneoBam, pCMV5neoBam-FLAG-PUMA or pCMV5neoBam-FLAG-PUMA W71A (PUMA$^{W\rightarrow A}$), allowed to recover for 24 h, treated with TNF (0, 5 and 10 ng/ml) and cycloheximide (10 μg/ml) for 6 hours and analyzed by AnnexinV-PE staining and flow cytometry for apoptosis. US9-GFP was cotransfected and only GFP positive cells were analyzed. **b**. *puma*$^{-/-}$ MEFs were transiently transfected with pCMVneoBam, pCMVneoBam-FLAG-PUMA or pCMVneoBam-FLAG-PUMA W71A (PUMA$^{W\rightarrow A}$), recovered for 24 h, treated with UV irradiation (0, 2.5 and 5 mJ/cm^2) and analyzed for apoptosis as above. **c**. Lysates from (**b**) were subjected to co-immunoprecipitation with anti-FLAG and analyzed by SDS-PAGE and western blot for FLAG-PUMA (wild type or W71A), BCL-xL and p53. Error bars in a and b represent the standard deviation calculated from at least three independent experiments. **d**. Schematic illustration of the mechanism by which PUMA induces unfolding within α2 and α3 of BCL-xL, which is associated with p53 release. The formation of a π-stacking interaction between His^{113} of BCL-xL (blue pentagon shapes) and Trp^{71} of PUMA (magenta geometric shapes) is associated with unfolding of α2 and α3 (α3* in the upper right). BCL-xL is represented as a multi-color hexagon, with the edges representing its α-helices, as marked, p53 as a yellow oval and PUMA in magenta in unbound form as a wavy line and as a cylinder when bound to BCL-xL.